Effect of the laser magnetic field on nonsequential double ionization of He, Li^+, and Be^{2+}

Erik Lötstedt* and Katsumi Midorikawa

Laser Technology Laboratory, RIKEN Advanced Science Institute, 2-1 Hirosawa, Wako, Saitama 351-0198, Japan

(Received 25 September 2012; published 24 January 2013)

The role of the magnetic field of the laser pulse and the importance of relativistic corrections to the equations of motion in the recollision double ionization of He, Li^+, and Be^{2+} are investigated within a classical trajectory model. It is found that the inclusion of the magnetic field is important even at intensities as low as 10^{15} W/cm^2, but that the relativistic corrections proportional to $1/c^2$ have no impact on either total probabilities or final momentum spectra. Two field configurations with counterpropagating pulses, previously proposed to circumvent the detrimental effect of the magnetic field on the double-ionization probability, are compared with the single-pulse case.

DOI: 10.1103/PhysRevA.87.013426 PACS number(s): 32.80.Rm, 34.80.Dp, 02.70.Uu

I. INTRODUCTION

The nonsequential double ionization (DI) of helium has since its discovery [1,2] attracted a lot of attention. Laser-driven helium has become an archetypal example of strong electron-electron correlation induced by an external laser field [3]. The ionization mechanism is intuitively explained in terms of recollision [4]: one electron pulled away from the atomic center is driven back to the core by the oscillating electric field to eject the second electron by a collision. In an alternative scenario, recollision excitation with subsequent ionization (RESI), the returning electron excites the second electron which is later ejected by tunneling [5].

Due to its importance as the simplest system exhibiting strong electron-electron correlation, laser-driven helium has been investigated from a number of different viewpoints. Experimentally, early measurements of the total DI yield exhibiting the famous "knee" structure [1,2] were followed by observations of differential electron momentum spectra [5–8], which led to the identification of different mechanisms of DI. A recent trend is to employ short pulses and exploit the sensitiveness of the electron spectra to the carrier-envelope phase [9].

Theoretically, different models have been employed to describe DI of He. These can be grouped into roughly four categories: (i) direct solution of the time-dependent Schrödinger equation [6,10], (ii) the strong-field approximation [11–13], (iii) classical trajectory models with some quantum mechanical elements [14,15], and (iv) purely classical models [16–19]. All have their advantages and drawbacks, offering different insights into the DI process. The latter two methods are attractive since they permit a direct and intuitive interpretation of the physical mechanisms involved in terms of the classical trajectories of the electrons.

In the present paper, we investigate one of the problems regarding DI of He and He-like ions which is still open: the importance of the magnetic field of the laser pulse. Usually, the laser pulse is approximated as an oscillating electric field, neglecting the magnetic field component. For laser wavelengths of $\lambda \approx 800$ nm, this is an excellent approximation for intensities of order 10^{15} W/cm^2 or less. However, the region where nonsequential DI of He has the largest yield occurs for intensities larger than 10^{15} W/cm^2 [2], even close to 10^{16} W/cm^2 in some theoretical models [20]. Considering a free electron at rest at the origin subjected to the laser field $\mathbf{E} = \hat{\mathbf{x}} E_0 \cos[\omega_0(t - z/c)]$, $\mathbf{B} = \hat{\mathbf{z}} \times \mathbf{E}$, one finds by solving the classical relativistic equations of motion that during one laser cycle this electron is moved an amount $\Delta z = (2\pi/c\omega_0)U_p$ in the propagation direction due to the Lorentz force of the magnetic field. Here ω_0 and E_0 are used to denote the angular frequency and peak electric field, respectively, of the laser field, $U_p = E_0^2/4\omega_0^2$ is the familiar ponderomotive potential, and c is the speed of light [all quantities are expressed in atomic units (a.u.)]. For 800 nm, 10^{16} W/cm^2 laser light, $\Delta z \approx 18$ a.u., which means that the effect of the magnetic field cannot be neglected in the description of recollision phenomena.

There exist only a few experiments addressing the above question [21–24], and the problem cannot be considered conclusively settled. A number of theoretical proposals [25–27] have been put forward to address the problem of the drift motion of the electron. To the best of our knowledge, these proposals have never been implemented in an experiment, neither have they been tested in realistic simulations involving several (more than one) electrons. For a recent investigation of the impact of the magnetic field on the ionization dynamics in a classical one-electron system, see [28]. We also mention the recent study [29] on the effect of an additional static magnetic field on DI of He. One of the difficulties of studying the above-mentioned topics is that there is currently no practical, microscopic theory of laser-driven relativistic many-particle dynamics. On the mean-field level, laser-driven relativistic plasmas are usually treated within the relativistic particle-in-cell scheme [30,31], but neither classical nor quantum simulations of laser-driven relativistic few-particle systems going beyond the mean-field description, allowing for collisions at small impact parameters, have so far appeared in the literature to the best of our knowledge.

The purpose of this contribution is twofold: (i) To investigate in detail the effect of the magnetic field of the laser pulse on the nonsequential DI process, within a model that explicitly treats the electron-electron correlation, and to assess quantitatively different methods to overcome the drift motion of the electron. Effects of the magnetic field are investigated for three cases: a single, few-cycle linearly polarized laser pulse, a setup with two delayed counterpropagating linearly polarized laser pulses proposed in [26], and two counterpropagating circularly polarized laser pulses, as proposed in [27]. (ii) To take the first steps towards a microscopic description

*loetstedte@riken.jp

of relativistic, laser-driven few-particle systems. Our model is a purely classical model of the three-body system consisting of two electrons and one nucleus, similar to the one used in [17,20,32]. We perform the simulations by solving numerically both the standard, nonrelativistic equations of motion as well as the equations of motion derived from the Darwin Lagrangian. The Darwin Lagrangian includes relativistic effects up to order $(v/c)^2$, where v is the magnitude of the velocity of the electron.

We proceed by introducing in Sec. II the theoretical model employed for the simulations. Details about the simulation procedure can be found in Sec. III. The results of the simulation, together with a discussion of the obtained spectra are presented in Secs. IV A (total probabilities) and IV B (momentum spectra). We conclude the paper in Sec. V.

II. THEORETICAL MODEL

Atomic units are used throughout the paper, unless otherwise specified. This implies that the mass and the magnitude of the charge of the electron equal unity, and that the numerical value of the speed of light is $c \approx 137$ a.u. The system considered consists of two electrons, labeled by $j = 1,2$, moving in the potential $V(\mathbf{r}-\mathbf{R})$ of a nucleus of charge number Z situated at $\mathbf{R}$, and the electric and magnetic field of a laser, denoted by $\mathbf{E}(t,\mathbf{r})$ and $\mathbf{B}(t,\mathbf{r})$. The nucleus is considered to have infinite mass, i.e., to be immobile. We conduct simulations based on the following equations of motion:

$$\frac{d\mathbf{r}_1}{dt} \equiv \mathbf{v}_1 = \mathbf{P}_1 - \frac{1}{2c^2}|\mathbf{P}_1|^2\mathbf{P}_1 - \frac{1}{2c^2}\frac{1}{|\mathbf{r}_{12}|}\left[\mathbf{P}_2 + \frac{(\mathbf{P}_2\cdot\mathbf{r}_{12})\mathbf{r}_{12}}{|\boldsymbol{r}_{12}|^2}\right], \tag{1a}$$

$$\frac{d\mathbf{P}_1}{dt} = \frac{\mathbf{r}_{12}}{|\mathbf{r}_{12}|^3} + \frac{1}{2c^2}\frac{1}{|\mathbf{r}_{12}|^3}\left[(\mathbf{P}_2\cdot\mathbf{r}_{12})\mathbf{P}_1 + (\mathbf{P}_1\cdot\mathbf{r}_{12})\mathbf{P}_2 - (\mathbf{P}_1\cdot\mathbf{P}_2)\mathbf{r}_{12} - 3(\mathbf{P}_1\cdot\mathbf{r}_{12})(\mathbf{P}_2\cdot\mathbf{r}_{12})\frac{\mathbf{r}_{12}}{|\mathbf{r}_{12}|^2}\right] - \boldsymbol{\nabla} V(\mathbf{r}_1-\mathbf{R}) - \mathbf{E}(t,\mathbf{r}_1) - \frac{\mathbf{v}_1}{c}\times\mathbf{B}(t,\mathbf{r}_1), \tag{1b}$$

$$\frac{d\mathbf{r}_2}{dt} \equiv \mathbf{v}_2 = \frac{d\mathbf{r}_1}{dt}(1\leftrightarrow 2), \tag{1c}$$

$$\frac{d\mathbf{P}_2}{dt} = \frac{d\mathbf{P}_1}{dt}(1\leftrightarrow 2), \tag{1d}$$

where we have used the notation $\mathbf{r}_{12} = \mathbf{r}_1 - \mathbf{r}_2$ and $\mathbf{r}_{21} = -\mathbf{r}_{12}$. The symbol $\mathbf{P}_j$ $(j = 1,2)$ appearing in Eq. (1) is the canonical momentum of the electron. The physical, kinetic momentum for electron j reads

$$\mathbf{p}_j = \mathbf{v}_j + \frac{\mathbf{v}_j^2}{2c^2}\mathbf{v}_j. \tag{2}$$

The equations of motion (1) can be derived from the Darwin Lagrangian L_D [33],

$$L_D = \sum_{j=1}^{2}\left[\frac{1}{2}\mathbf{v}_j^2 + \frac{1}{8c^2}\mathbf{v}_j^4 + V(\mathbf{r}_j-\mathbf{R}) - \frac{\mathbf{v}_j}{c}\cdot\mathbf{A}(t,\mathbf{r}_j)\right] - \frac{1}{|\mathbf{r}_{12}|} + \frac{1}{2c^2}\frac{1}{|\mathbf{r}_{12}|}\left[\mathbf{v}_1\cdot\mathbf{v}_2 + \frac{(\mathbf{v}_1\cdot\mathbf{r}_{12})(\mathbf{v}_2\cdot\mathbf{r}_{12})}{|\mathbf{r}_{12}|^2}\right], \tag{3}$$

where $\mathbf{A}(t,\mathbf{r})$ is the vector potential of the laser field. The Lagrangian L_D includes relativistic effects up to order v^2/c^2, and is valid for velocities much smaller than the speed of light, $v \ll c$. In terms of the motion of an electron in a laser wave, the condition $v \ll c$ translates into $E_0/\omega_0 \ll c$ for the laser field amplitude and frequency (expressed in a.u.), or $I \ll 2\times 10^{18}$ W/cm^2 for the intensity in the case of 800 nm laser light. To describe first-order relativistic effects, the Darwin Lagrangian is convenient, since the time derivatives of the positions and canonical momenta at time t are functions of the positions and momenta at the same time t. In a completely relativistic description, this would not be possible due to retardation, i.e., the force on a particle at one instant depends on the positions of the other particles at an earlier instant. We note that the Darwin approximation has been suggested previously as a tool for plasma simulation [34], but we are unaware of its application to laser-driven atomic systems.

In the following, we present results obtained at three different levels of approximation: (i) Nonrelativistic approximation (referred to in the following as NRA); here terms proportional to c^{-1} or c^{-2} are neglected in (1), which means that there is no force due to the magnetic field. (ii) Nonrelativistic approximation with a magnetic field (referred to as NRBA); in this case, all terms proportional to c^{-2} in (1) are discarded. However, we keep the magnetic field term $(\mathbf{v}/c)\times\mathbf{B}$ in the Lorentz force. (iii) Darwin approximation (referred to as DA); the full equations of motion given by Eq. (1) are solved.

Since the model we use is entirely classical, a bare Coulomb potential cannot be used for the nuclear potential. We employ the standard soft-core potential [17]

$$V(\mathbf{r}) = -\frac{Z}{\sqrt{\mathbf{r}^2+\alpha^2}}. \tag{4}$$

The softening parameter α is set such that autoionization of the ground state does not occur (which imposes a lower bound on α), and such that the energy of the lowest-energy configuration of the two electrons is below the ground-state energy $\epsilon_0(Z)$ of the corresponding atom or ion (this puts an upper bound on α). To fix $\epsilon_0(Z)$, we use the approximate quantum mechanical formula for the ground-state energy of He and He-like ions in [35]. The numerical values (in a.u.) for the parameter pairs (ϵ_0,α) employed in the following read

$$(\epsilon_0,\alpha) = \begin{cases} (-2.904, 0.7918) & \text{if } Z = 2, \\ (-7.280, 0.5060) & \text{if } Z = 3, \\ (-13.66, 0.3730) & \text{if } Z = 4. \end{cases} \tag{5}$$

III. SIMULATION

The simulations are carried out in a statistical, Monte Carlo fashion, which is a well-established method for laser-atom interaction [16,32,36]. First, initial values for the canonical momenta and positions are sampled by a procedure described in some detail below. Then the equations of motion given by (1) are integrated numerically by an adaptive, fifth-order Runge-Kutta solver. At a sufficiently long time after the laser pulse has passed, the ionization state (doubly ionized, singly ionized, or not ionized) and final momenta of the electrons are recorded. An electron j is considered to be ejected if its energy

$\varepsilon_j > 0$, where the single-electron energy is defined as

$$\varepsilon_j = \frac{\mathbf{v}_j^2}{2} + \frac{3\mathbf{v}_j^4}{8c^2} + V(\mathbf{r}_j - \mathbf{R}) + \frac{1}{2}\left[\frac{1}{|\mathbf{r}_{12}|} + \frac{1}{2c^2|\mathbf{r}_{12}|}\left(\mathbf{v}_1\cdot\mathbf{v}_2 + \frac{(\mathbf{v}_1\cdot\mathbf{r}_{12})(\mathbf{v}_2\cdot\mathbf{r}_{12})}{|\mathbf{r}_{12}|^2}\right)\right]. \quad (6)$$

Here we have adopted the convention that the parts of the total energy ϵ that depend on the coordinates and velocities of both electrons are split equally between the two electrons. The total energy then satisfies $\epsilon = \varepsilon_1 + \varepsilon_2$. Obviously, the terms proportional to c^{-2} in Eq. (6) are relevant only in the DA.

The initial values for the electrons are sampled in the following way. First, the electrons are placed at $\mathbf{r}_1 = r_{\rm eq}\hat{\mathbf{r}}_{\rm rand}$, $\mathbf{r}_2 = -\mathbf{r}_1$, where $r_{\rm eq} = \alpha/\sqrt{(4Z)^{2/3} - 1}$ is the equilibrium distance for two electrons in a soft-core potential, and $\hat{\mathbf{r}}_{\rm rand}$ is a random unit vector. In this configuration, the total energy ϵ of the system is less than $\epsilon_0(Z)$ given in Eq. (5). Second, a total amount $\epsilon_0(Z) - \epsilon$ of kinetic energy is added to the system in the form of momentum, directed along either $\mathbf{r}_1$ or $\mathbf{r}_2$, and randomly split between the two electrons. This implies that the initial configuration has vanishing total angular momentum. Third, the system is allowed to evolve for 100 a.u. of time before the interaction with the laser pulse. We use the same set of initial conditions for all three approximations, the NRA, NRBA, and DA. The above described method of initial value sampling can be considered to be a commonly accepted procedure [16,32]. If not otherwise stated, the nucleus is placed at the origin, $\mathbf{R} = \mathbf{0}$.

Three different laser field configurations, labeled SL, CL, and CC, are used in the simulations. The first (configuration SL) corresponds to a single, few-cycle linearly polarized laser pulse with a sine-squared envelope propagating in the z direction,

$$\mathbf{E}_{\rm SL}(t,\mathbf{r}) = E_0\cos(\omega_0\eta_-)\sin^2\left(\frac{\pi\eta_-}{T}\right)b_0^T(\eta_-)\hat{\mathbf{x}},$$
$$\mathbf{B}_{\rm SL}(t,\mathbf{r}) = \hat{\mathbf{z}}\times\mathbf{E}_{\rm SL}(t,\mathbf{r}), \quad (7)$$

where $\eta_- = t - z/c$, $T = 2\pi N/\omega_0$ is the total pulse duration, and $b_{t_0}^{t_1}(\cdot)$ is the box function, defined as $b_{t_0}^{t_1}(t) = 1$ when $t_0 \leqslant t \leqslant t_1$, and 0 otherwise. Throughout this paper, we take $N = 3$ as the number of cycles, and $\omega_0 = 0.057$ a.u., which corresponds to a wavelength of 800 nm.

The second laser field configuration, denoted by CL, corresponds to the setup proposed in [26],

$$\mathbf{A}_{\rm CL}(t,\mathbf{r}) = -\hat{\mathbf{x}}\frac{E_0 c}{\omega_0}\cos(\omega_0\eta_-)\sin^2\left(\frac{\pi\eta_-}{T}\right)b_0^T(\eta_-) - \hat{\mathbf{x}}\frac{\sqrt{2}E_0 c}{\omega_0}\cos(\omega_0\eta_+)\sin^2\left(\frac{\pi\eta_+}{T}\right)b_T^{2T}(\eta_+),$$
$$\mathbf{E}_{\rm CL}(t,\mathbf{r}) = -\frac{1}{c}\frac{\partial}{\partial t}\mathbf{A}_{\rm CL}(t,\mathbf{r}), \quad \mathbf{B}_{\rm CL}(t,\mathbf{r}) = \nabla\times\mathbf{A}_{\rm CL}(t,\mathbf{r}), \quad (8)$$

where $\eta_+ = t + z/c$. The total laser field thus consists of two consecutive, counterpropagating laser pulses of linear polarization, the second one with twice the peak intensity of the first. An electron at rest at the origin at $t = 0$ is first driven away in the positive z direction by the first pulse, and then pushed back by the second pulse to return to the origin at maximal kinetic energy [26].

The third setup, labeled by CC, is that put forward in [27],

$$\mathbf{E}_{\rm CC}(t,\mathbf{r}) = E_0 b_0^T(\eta_-)\sin^2\left(\frac{\pi\eta_-}{T}\right)[\cos(\omega_0\eta_-)\hat{\mathbf{x}} + \sin(\omega_0\eta_-)\hat{\mathbf{y}}] + E_0 b_0^T(\eta_+)\sin^2\left(\frac{\pi\eta_+}{T}\right)\times[\cos(\omega_0\eta_+)\hat{\mathbf{x}} - \sin(\omega_0\eta_+)\hat{\mathbf{y}}],$$
$$\mathbf{B}_{\rm CC}(t,\mathbf{r}) = E_0 b_0^T(\eta_-)\sin^2\left(\frac{\pi\eta_-}{T}\right)[\cos(\omega_0\eta_-)\hat{\mathbf{y}} - \sin(\omega_0\eta_-)\hat{\mathbf{x}}] - E_0 b_0^T(\eta_+)\sin^2\left(\frac{\pi\eta_+}{T}\right)\times[\cos(\omega_0\eta_+)\hat{\mathbf{y}} + \sin(\omega_0\eta_+)\hat{\mathbf{x}}], \quad (9)$$

two counterpropagating circularly polarized laser pulses of equal intensity. In this setup, the Lorentz forces in the z direction mutually cancel, so that the probability for recollision is enhanced. However, for a finite pulse such as described by Eq. (9), this condition holds strictly only at $z = 0$.

For the three field configurations SL, CL, and CC, we conduct simulations at various peak field strengths E_0. When results are displayed as a function of the laser intensity I, we use the formula $I\ ({\rm W/cm^2}) = 3.51\times10^{16}E_0^2$ (a.u.) for the conversion.

IV. RESULTS

A. Total probabilities

In Figs. 1 and 2 we show the results for the total probability for DI of He and Li^+, defined as $P_{\rm DI} = n_{\rm DI}/n_{\rm tot}$. Here $n_{\rm DI}$ is the number of trajectories which resulted in both electrons being unbound ($\varepsilon_j > 0$, $j = 1,2$) at the end of the trajectory. The total number of trajectories run at each intensity were $n_{\rm tot} \approx 1.3\times10^6$ for $Z = 2$ and $n_{\rm tot} \approx 9\times10^5$ for $Z = 3$.

Several remarks can be made based on Figs. 1 and 2. Although the plateau structure of the total probability for DI of He with a single pulse [Fig. 1(a)] stretches up to as far as $I = 10^{16}$ W/cm^2 in this model, inclusion of the magnetic field reduces the height of the plateau only by a factor $\approx$2. For DI of Li^+ [$Z = 3$, Fig. 2(a)], inclusion of the magnetic field reduces the single-pulse plateau probabilities by an order of magnitude. This reduction of the plateau height is only marginally smaller for the field configuration CL, the linearly polarized double pulse, for both He and Li^+, which can be seen in Figs. 1(b) and 2(b). On the contrary, field configuration CC, the counterpropagating circularly polarized pulses, results in equal DI probabilities with and without magnetic field for both He [Fig. 1(c)] and Li^+ [Fig. 2(c)].

For both He and Li^+, regardless of the field configuration employed, we could not find any difference between the results obtained in the DA and the NRBA. In principle, since a field-driven system of two charged particles in a binding potential is chaotic, i.e., the final outcome is extremely sensitive to variations in the initial conditions, even a small modification of the Hamiltonian of the system [such as the terms proportional to c^{-2} in (1)] could lead to observable

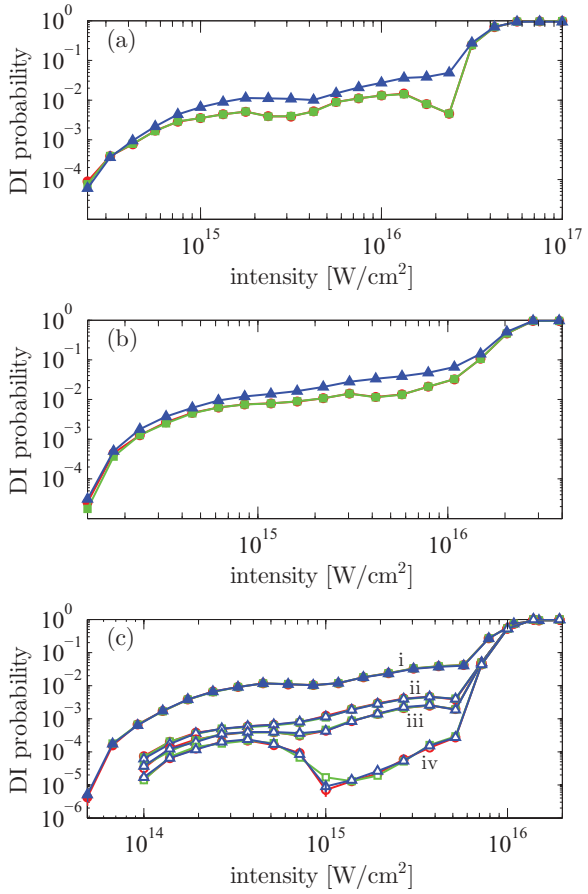

FIG. 1. (Color online) Probability for DI of He ($Z = 2$) as a function of the laser intensity, for the different field configurations. Field configuration (a) SL [a single linearly polarized pulse, see Eq. (7)], (b) CL [two counterpropagating linearly polarized pulses, see Eq. (8)], and (c) CC [two counterpropagating circularly polarized pulses, see Eq. (9)]. $\mathbf{R} = \mathbf{0}$ in (a) and (b). The different curve styles correspond to the different approximations of the equations of motion: NRA, solid triangles; NRBA, solid squares; and DA, solid circles. In all panels the NRBA and DA curves are almost indistinguishable, and in (c) all three curves lie almost on top of each other. In (c), in addition to the curves obtained at $R_z = 0$ (solid symbols, marked with i), we also show curves calculated at $R_z \neq 0$ (open symbols), $R_z = 1$ a.u., (ii); $R_z = 200$ a.u., (iii); and $R_z = 1000$ a.u., (iv).

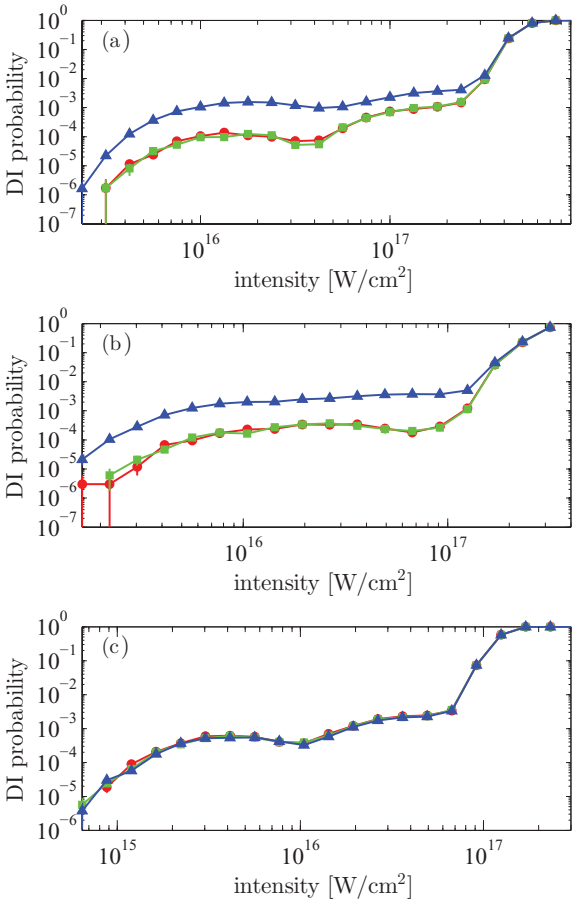

FIG. 2. (Color online) Probability for DI of Li^+ ($Z = 3$) as a function of the laser intensity, for the different field configurations. Field configuration (a) SL, (b) CL, and (c) CC. $\mathbf{R} = \mathbf{0}$ in all panels. The different curve styles correspond to the different approximations of the equations of motion: NRA, solid triangles; NRBA, solid squares; and DA, solid circles. Statistical error bars $\pm\sqrt{n_{\rm DI}}/n_{\rm tot}$ are shown when their lengths exceed the size of the curve symbol.

differences in the final probabilities or spectra. Moreover, the terms in (1) proportional to $P_1 P_2/(c^2 r_{12}^2)$ could become significant for large momenta and small electron separation, as is the case at a recollision. However, no statistically significant difference between including or excluding the c^{-2} terms was found in the present investigation. We do observe the sensitiveness of the initial conditions in the sense that exactly the same initial positions and momenta that lead to DI in the DA do not necessarily lead to DI in the NRBA. For example, when we use a set of initial conditions which all lead to DI in the DA case for $I = 2 \times 10^{15}$ W/cm^2, field configuration SL [the set of initial conditions that produces trajectories with final momentum spectrum shown in Fig. 5(c)], and repeat the simulation in the NRBA, only 20% of the trajectories result in DI. Nevertheless, when averaged over many trajectories run from slightly different initial conditions, the DA and NRBA models give the same results, within the statistical error bars. The same conclusion is arrived at also in Sec. IV B, where the momentum distribution of the two ejected electrons is analyzed. To the contrary, the inclusion or not of the magnetic field, which can be viewed as a zeroth-order compared to a first-order approximation in c^{-1}, affects the final probabilities and momentum spectra (as will be seen in Sec. IV B) in a quantitatively significant way.

For field configuration CC and $Z = 2$, we have also investigated the dependence of the total DI probability on the position $\mathbf{R}$ of the nucleus. In Fig. 1(c), we show the results obtained at four different values of R_z, with $\mathbf{R} = (0,0,R_z)$. This figure reveals the sensitivity of the DI probability to the displacement of the He atom along the laser pulse propagation axis for field configuration CC. Already a small displacement of 1 a.u. from the laser focus reduces the DI probability by almost one order of magnitude. This reduction is because the polarization of the total pulse (9) effectively becomes slightly elliptical at $R_z \neq 0$. It should be noted that the laser pulse (9) is only an approximation to the electric and magnetic fields of a focused laser pulse, which cannot be described by a plane wave in general. However, close to the focal region, even a

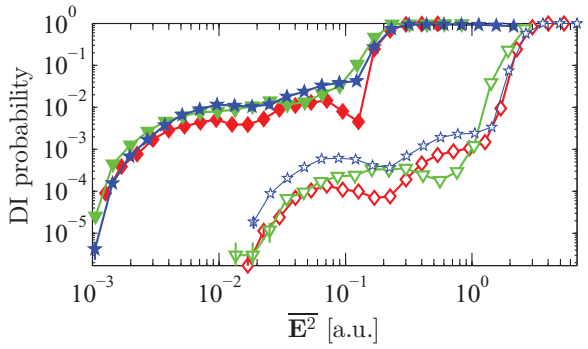

FIG. 3. (Color online) Probability for DI of He (solid symbols) and Li^+ (open symbols) as a function of the average intensity $\overline{\mathbf{E}^2}$ [see Eq. (10)], in the DA. $\mathbf{R} = \mathbf{0}$ for all curves. Results for field configuration SL are shown with diamonds, for CL with inverted triangles, and for CC with stars.

focused pulse is well approximated by a plane wave of the form (9).

To conclude the presentation of the $Z = 2$ and $Z = 3$ results, we compare in Fig. 3 the total DI probabilities in the DA for He and Li^+ (i.e., the same data points as shown with solid circles in Figs. 1 and 2). We plot the total DI probabilities as a function of the average intensity $\overline{\mathbf{E}^2}$, defined here as

$$\overline{\mathbf{E}_a^2} = \frac{1}{\tau_a}\int_0^\infty [\mathbf{E}_a(t,\mathbf{0})]^2 dt, \tag{10}$$

where a = SL, CL, or CC, and the total pulse length $\tau_{\mathrm{SL,CC}} = T$ and $\tau_{\mathrm{CL}} = 2T$. For a realistic, finite pulse, $\overline{\mathbf{E}^2}$ would be proportional to the total pulse energy. Note, however, that for plane-wave pulses considered in this paper, the total pulse energy is not defined. From Fig. 3, we see that field configuration CC is superior (although the difference is small for He), in the sense that this field configuration yields the highest DI probability at a given average intensity.

We have also conducted simulations for the He-like ion Be^{2+} ($Z = 4$), but only for field configuration SL. The results are shown in Fig. 4. About $n_{\mathrm{tot}} \approx 5 \times 10^6$ trajectories were

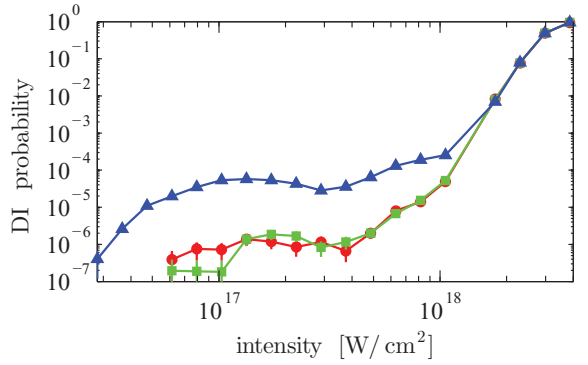

FIG. 4. (Color online) Probability for DI of Be^{2+} ($Z = 4$) as a function of the laser intensity, for field configuration SL, a single few-cycle pulse [see Eq. (7)]. $\mathbf{R} = \mathbf{0}$. The different curve styles correspond to the different approximations of the equations of motion: NRA, solid triangles; NRBA, solid squares; and DA, solid circles. Statistical error bars $\pm\sqrt{n_{\mathrm{DI}}}/n_{\mathrm{tot}}$ are shown when their lengths exceed the size of the curve symbol.

calculated at each intensity. The difference in probability between the NRA and the NRBA and DA results is here almost two orders of magnitude in the plateau region. Also note the high laser intensities needed for DI. Strictly speaking, the DA breaks down at the higher end of the intensity range considered in Fig. 4, since at $I \approx 10^{18}$ W/cm^2 the condition $v \ll c$ is no longer satisfied. To explore even higher values of Z, a fully relativistic model would be required.

It may seem from Fig. 4 that the DA and NRBA curves are different. Due to the low probability, however, the points on the DA and NRBA curves in Fig. 4 in the plateau region ($I \approx 10^{17}$ W/cm^2) result from only a few DI trajectories, which makes it difficult to make any statistically significant conclusions. We have therefore repeated the simulations for $Z = 4$ at one particular intensity $I = 2 \times 10^{17}$ W/cm^2, with field configuration SL (as in Fig. 4), and increased the total number of simulated trajectories. From $n_{\mathrm{tot}} \approx 10^8$ trajectories run, we get $P_{\mathrm{DI}}^{(\mathrm{DA})} = (1.76 \pm 0.13) \times 10^{-6}$, and $P_{\mathrm{DI}}^{(\mathrm{NRBA})} = (1.70 \pm 0.13) \times 10^{-6}$ for the DI probabilities, where we have also indicated the estimated statistical error. We conclude that even at $Z = 4$, $I = 2 \times 10^{17}$ W/cm^2 the DA and NRBA give indistinguishable results within the statistical uncertainties.

B. Momentum distributions

In this section we show examples of the correlated momentum spectra of the ejected electrons. The first example of the final momentum distribution in the x direction is displayed in Fig. 5, which contains the results of a simulation made at $I = 2 \times 10^{15}$ W/cm^2, with field configuration SL (single linearly polarized pulse). The x direction here corresponds to the polarization direction of the electric field. We first remark that, similarly to the results for the total DI probability presented in Sec. IV A, there is no difference between the NRBA distribution [Fig. 5(b)] and the DA distribution [Fig. 5(c)], apart from statistical fluctuations.

On the contrary, comparing Fig. 5(a) and Fig. 5(b) [or Fig. 5(c)], we see that the magnetic field has a large impact on the momentum distribution. In the NRBA and DA spectra, the ridge ranging from $(p_{1x}, p_{2x}) \approx (-4,0)$ a.u. to $(p_{1x}, p_{2x}) \approx (0,-4)$ a.u. clearly seen in the NRA spectrum is almost completely absent. After a trajectory analysis, we find that two classes of trajectories give rise to the features exhibited by the NRA momentum distribution in Fig. 5(a). The first is the trajectory in which the electron ejected at one field maximum returns to eject the second electron approximately one half cycle later. This kind of trajectory results in at least one of the ejected electrons having positive final momentum in the x direction, and the other one positive or slightly negative p_x. This feature is common to all three panels in Fig. 5. An example of such a trajectory, calculated in the NRA, is displayed in Fig. 6(a). One electron is ejected close to the first peak of the laser pulse and recollides a half cycle later at the next peak.

The second class of trajectories are the long ones, where the ejected electron returns after an almost complete field cycle to eject the second electron. A typical trajectory of this kind is shown in Fig. 6(b). These trajectories give rise to the ridge seen in Fig. 5(a) in the lower left quadrant of the p_{1x}-p_{2x} plane. The explanation of why this ridge is absent for the NRBA and DA calculations is simply that the long trajectories are much less

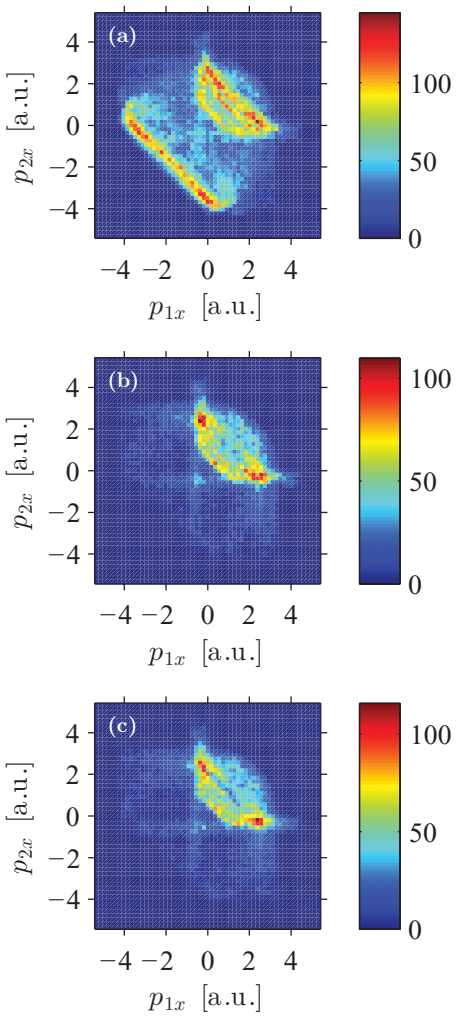

FIG. 5. (Color online) Final distribution of the electron momenta p_{1x} and p_{2x} in the x direction (polarization direction) in DI of He, for a single, three-cycle pulse (field configuration SL) of intensity 2×10^{15} W/cm^2. $\mathbf{R} = \mathbf{0}$. Results employing the NRA are shown in (a), NRBA in (b), and DA in (c). The color indicates the number of trajectories with final momentum in that particular bin. In total $n_{\text{tot}} = 5 \times 10^6$ trajectories were run.

probable if the magnetic field is included, due to the tendency of the $(\mathbf{v}/c) \times \mathbf{B}$ force to prevent the ejected electron from recolliding.

We note that the above analysis of the dynamics using long and short trajectories is similar to that introduced in order to understand high-harmonic generation [37].

We now proceed to show in Fig. 7 the correlated final p_{1x}-p_{2x} spectrum for Li^+, at $I = 1 \times 10^{17}$ W/cm^2, field configuration SL. The NRBA [Fig. 7(b)] and DA [Fig. 7(c)] distributions cannot be distinguished, which shows that even at high laser intensity the c^{-2} terms in the equations of motion (1) are unimportant also for the momentum spectra.

For the NRBA and DA distributions, there are two main features, both of which are present also in the NRA case. The first is the peak in the lower left quadrant of the p_{1x}-p_{2x} plane, where both electrons have the same final momenta $p_{1x} = p_{2x} \approx -11$ a.u. This peak corresponds to a genuine recollision: an electron ejected during the first laser cycle recollides

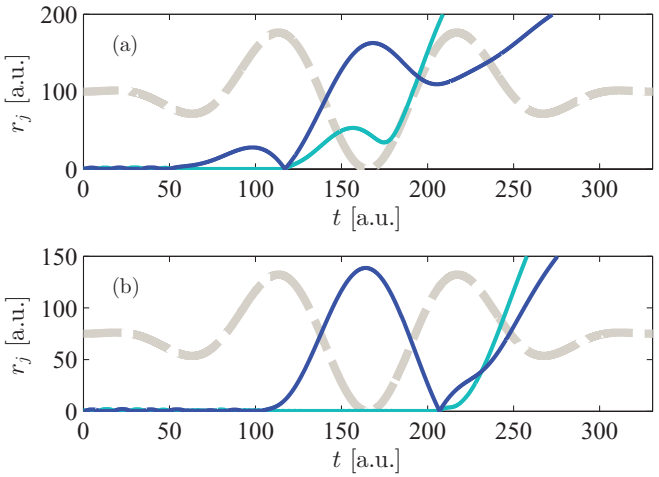

FIG. 6. (Color online) Two examples of DI trajectories contributing to the different features of the momentum spectrum. The distance $r_j(t) = |\mathbf{r}_j(t)|$ from the nucleus for each electron $j = 1,2$ is shown with a solid line. The time development of the x component of the laser electric field $\hat{\mathbf{x}} \cdot \mathbf{E}_{\text{SL}}(t,\mathbf{0})$ is shown with a thicker, broken line (not to scale, and vertically shifted). All parameters are the same as used for the results shown in Fig. 5(a): NRA, field configuration SL, laser intensity 2×10^{15} W/cm^2, and $\mathbf{R} = \mathbf{0}$. In (a), the final momenta are $(p_{1x}, p_{2x}) = (2.2, -0.13)$ a.u., while in (b) we have $(p_{1x}, p_{2x}) = (-2.4, -0.84)$ a.u.

with the remaining electron at a small impact parameter, and transfers roughly half of its momentum to the second electron, after which both electrons promptly escape from the nucleus with roughly the same kinetic energy. The recollision occurs at $t_0 \approx 95$ a.u., shortly before the end of the first field cycle, which fixes the final momentum as $p_{1x} = p_{2x} \approx -\int_{t_0}^{T} \hat{\mathbf{x}} \cdot \mathbf{E}_{\text{SL}}(t,\mathbf{0}) dt \approx -11$ a.u. In Fig. 8(a), an example from this group of trajectories is demonstrated. Note that the time from ejection to recollision is shorter than a half cycle.

The second main feature is the two stripes (one horizontal, and one vertical), where one of the electrons ($j = 1$ or 2) has final momentum $-13 \leqslant p_{jx} \leqslant -11$ a.u., and the other electron has final momentum $p_{(3-j)x}$ in the range -11 to approximately 15 a.u. In this case, the final momenta are uncorrelated. The trajectories leading to this feature are of the RESI type [3]: one electron is ejected during the peak of the first cycle, and then recollides after less than a half cycle later. After recollision, only one electron is ejected, whereas the second one is left bound in an excited state, and is ejected at a later time by field ionization. The recolliding electron either excites the bound electron and scatters, or ejects the bound electron and recombines into a transient bound state, so that the electron that is emitted directly after the recollision event is not necessarily the one that was first ejected. Both types of trajectories contribute to the horizontal and vertical stripes in the momentum distributions in Fig. 7. We refer to Fig. 8(b) for an example of a trajectory where the recolliding electron is recaptured into an excited state and ejected during a subsequent field maximum. Note that since the laser field is very intense, the ejection of the second electron is not limited to a field maximum, which explains the range of possible final momenta for the second electron.

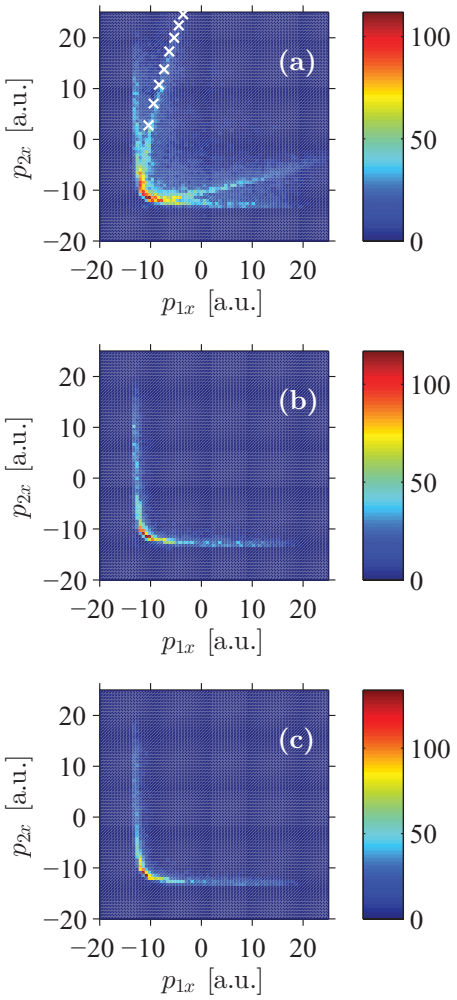

FIG. 7. (Color online) Final distribution of the electron momenta p_{1x} and p_{2x} in the x direction (polarization direction), for field configuration SL, in DI of Li^+ at intensity 1×10^{17} W/cm^2. $\mathbf{R} = \mathbf{0}$. Results for the NRA are shown in (a), NRBA in (b), and DA in (c). In (a), final momenta obtained from the approximation (11) are shown with white crosses (×). A total number of $n_{\rm tot} = 1.2 \times 10^7$ trajectories were run for each plot.

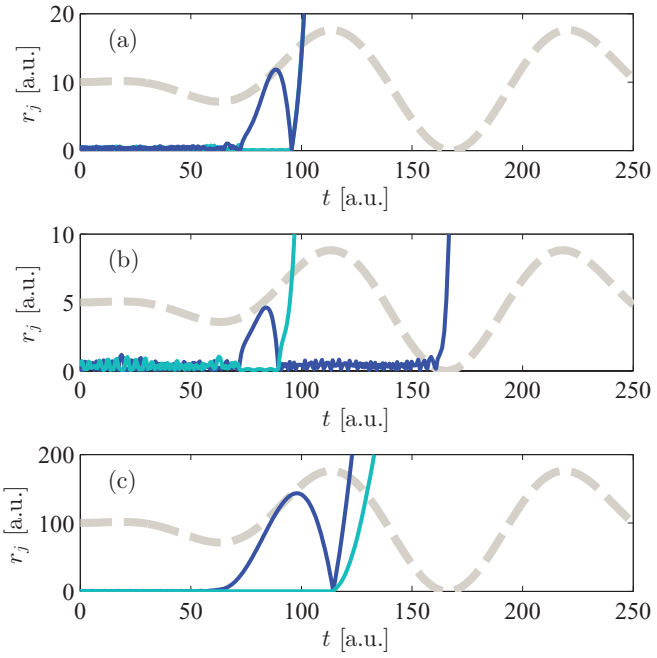

FIG. 8. (Color online) Trajectories $r_{1,2}(t)$ contributing to the momentum spectra shown in Fig. 7 are drawn with solid lines. For orientation, the x component of the laser electric field (not to scale, and vertically shifted) is shown with a broken line. The laser intensity is $I = 1 \times 10^{17}$ W/cm^2, the field configuration is SL, $Z = 3$, and $\mathbf{R} = \mathbf{0}$ (the same parameters as employed in Fig. 7). In (a), the final momenta are $(p_{1x}, p_{2x}) = (-11.0, -11.3)$ a.u., in (b) we have $(p_{1x}, p_{2x}) = (2.7, -12.7)$ a.u., and in (c) $(p_{1x}, p_{2x}) = (-7.5, 10.0)$ a.u. The DA was used in (a) and (b), and the NRA in (c). Note that in (a), the two curves almost overlap each other after the recollision at $t \approx 95$ a.u.

Left to discuss is the part of the final momentum distribution which can be seen in the NRA plot [Fig. 7(a)], but not in the NRBA or DA plot. The part of this feature which has $p_{1x} < 0$ is marked with crosses in Fig. 7(a). The corresponding trajectories in this case are soft recollisions at large impact parameter, so that the recolliding electron transfers only a small part of its relatively large momentum to the bound electron. The time between ejection and recollision is here close to one half cycle, rather long compared to the two classes of trajectories discussed above. A typical trajectory is shown in Fig. 8(c). The longer time for recollision together with the soft nature of the recollision makes this kind of trajectory extremely unlikely if the magnetic field is included, which explains the absence of this feature in Figs. 7(b) and 7(c). Assuming that the ejection of electron 1 occurs at $t = t_1$, we can estimate the time t_2 for the recollision as the smallest $t_2 > t_1$ for which the equation $\int_{t_1}^{t_2} dt \int_{t_1}^{t} \hat{\mathbf{x}} \cdot \mathbf{E}_{\rm SL}(t', \mathbf{0}) dt' = 0$ is satisfied. Since the momentum transfer in the recollision is small, the final momenta of the electrons can be approximated as

$$p_{jx} \approx -\int_{t_j}^{T} \hat{\mathbf{x}} \cdot \mathbf{E}_{\rm SL}(t, \mathbf{0}) dt, \tag{11}$$

for $j = 1,2$. The approximation (11) for p_{1x} and p_{2x}, with $50 \leqslant t_1 \leqslant 67$ a.u., is shown in Fig. 7(a) with crosses.

V. CONCLUSIONS

In this paper, we have addressed two open questions regarding the DI of He and He-like ions: the importance of including the magnetic field of the laser pulse in the simulation and the impact of second-order (in $1/c$) corrections to the equations of motion. It was found that the magnetic field can have substantial influence on both the total DI probability and on the final momentum spectrum, even at laser intensities as low as 10^{15} W/cm^2, which is commonly thought of as a nonrelativistic intensity (at 800 nm wavelength). On the other hand, the $1/c^2$ corrections, as derived from the Darwin Lagrangian, were shown to have a negligible effect on the total probabilities and final momentum spectra, even for Be^{2+} driven by 2×10^{17} W/cm^2 laser light. The reason is that at high laser intensities, the trajectories that lead to DI by recollision occur exclusively during the first cycle of the pulse, when the field is still relatively weak.

In order to increase the DI probability, three field configurations were implemented and assessed in the simulations.

Two of these were proposed previously [26,27] as suitable setups to allow for DI even at relativistically strong laser fields where the $\mathbf{v} \times \mathbf{B}$ force generally impedes recollision. We conclude that the setup with two counterpropagating circularly polarized laser pulses proposed in [27] is superior, since the DI probability of Li^+ increases by almost one order of magnitude in the plateau region (see Fig. 3). However, as shown in Fig. 1(c), in the current setup with short pulses, the DI probability is very sensitive to the displacement of the atom (or ion) along the laser focus. This fact severely restricts the practical applicability of this setup.

The model employed in the current investigation is classical. To investigate the large-amplitude motion of strongly driven electrons, classical models are convenient, since one is not restricted to finite-sized grids as in the case of the numerical solution of the Schrödinger equation. Moreover, within the classical model employed, electron-electron correlation can be treated without approximations. To be able to compare the total probabilities and final spectra quantitatively with experimental data, quantum tunneling has to be included. However, at the charge numbers ($Z \leqslant 4$) and intensities ($I \leqslant 10^{18}$ W/cm^2) considered in this paper, the tunneling process itself is essentially nonrelativistic [38]. We therefore expect the conclusions about the recollision dynamics reached in this paper to be valid also in the quantum case.

ACKNOWLEDGMENTS

E.L. is supported by the FPR program of RIKEN, and acknowledges allocation of computing resources on the RIKEN Integrated Cluster of Clusters (RICC) system (Project No. Q12263).

[1] D. N. Fittinghoff, P. R. Bolton, B. Chang, and K. C. Kulander, Phys. Rev. Lett. **69**, 2642 (1992).
[2] B. Walker, B. Sheehy, L. F. DiMauro, P. Agostini, K. J. Schafer, and K. C. Kulander, Phys. Rev. Lett. **73**, 1227 (1994).
[3] C. Figueira de Morisson Faria and X. Liu, J. Mod. Opt. **58**, 1076 (2011).
[4] P. B. Corkum, Phys. Rev. Lett. **71**, 1994 (1993).
[5] B. Feuerstein, R. Moshammer, D. Fischer, A. Dorn, C. D. Schröter, J. Deipenwisch, J. R. Crespo Lopez-Urrutia, C. Höhr, P. Neumayer, J. Ullrich, H. Rottke, C. Trump, M. Wittmann, G. Korn, and W. Sandner, Phys. Rev. Lett. **87**, 043003 (2001).
[6] J. S. Parker, B. J. S. Doherty, K. T. Taylor, K. D. Schultz, C. I. Blaga, and L. F. DiMauro, Phys. Rev. Lett. **96**, 133001 (2006).
[7] Y. Liu, S. Tschuch, A. Rudenko, M. Dürr, M. Siegel, U. Morgner, R. Moshammer, and J. Ullrich, Phys. Rev. Lett. **101**, 053001 (2008).
[8] Y. Liu, D. Ye, J. Liu, A. Rudenko, S. Tschuch, M. Dürr, M. Siegel, U. Morgner, Q. Gong, R. Moshammer, and J. Ullrich, Phys. Rev. Lett. **104**, 173002 (2010).
[9] B. Bergues, M. Kübel, N. G. Johnson, B. Fischer, N. Camus, K. J. Betsch, O. Herrwerth, A. Senftleben, A. Max Sayler, T. Rathje, T. Pfeifer, I. Ben-Itzhak, R. R. Jones, G. G. Paulus, F. Krausz, R. Moshammer, J. Ullrich, and M. F. Kling, Nat. Commun. **3**, 813 (2012).
[10] Q. Liao, Y. Zhou, C. Huang, and P. Lu, New J. Phys. **14**, 013001 (2012).
[11] A. Becker and F. H. M. Faisal, Phys. Rev. Lett. **84**, 3546 (2000).
[12] S. V. Popruzhenko, P. A. Korneev, S. P. Goreslavski, and W. Becker, Phys. Rev. Lett. **89**, 023001 (2002).
[13] C. F. Faria, X. Liu, A. Sanpera, and M. Lewenstein, Phys. Rev. A **70**, 043406 (2004).
[14] X. Liu and C. Figueira de Morisson Faria, Phys. Rev. Lett. **92**, 133006 (2004).
[15] H. Li, J. Chen, H. Jiang, J. Liu, P. Fu, Q. Gong, Z.-C. Yan, and B. Wang, Opt. Express **16**, 20562 (2008).
[16] P. J. Ho, R. Panfili, S. L. Haan, and J. H. Eberly, Phys. Rev. Lett. **94**, 093002 (2005).
[17] S. L. Haan, J. S. Van Dyke, and Z. S. Smith, Phys. Rev. Lett. **101**, 113001 (2008).
[18] F. Mauger, C. Chandre, and T. Uzer, Phys. Rev. Lett. **104**, 043005 (2010).
[19] B. Yu, D. Zhang, Y. Li, and Q. Tang, J. Mod. Opt. **59**, 679 (2012).
[20] S. L. Haan, Z. S. Smith, K. N. Shomsky, P. W. Plantinga, and T. L. Atallah, Phys. Rev. A **81**, 023409 (2010).
[21] N. Ekanayake, B. L. Wen, L. E. Howard, S. J. Wells, M. Videtto, C. Mancuso, T. Stanev, Z. Condon, S. LeMar, A. D. Camilo, R. Toth, M. F. Decamp, and B. C. Walker, J. Phys. B **44**, 045604 (2011).
[22] S. Palaniyappan, R. Mitchell, R. Sauer, I. Ghebregziabher, S. L. White, M. F. Decamp, and B. C. Walker, Phys. Rev. Lett. **100**, 183001 (2008).
[23] S. Palaniyappan, A. DiChiara, I. Ghebregziabher, E. L. Huskins, A. Falkowski, D. Pajerowski, and B. C. Walker, J. Phys. B **39**, S357 (2006).
[24] S. Palaniyappan, A. DiChiara, E. Chowdhury, A. Falkowski, G. Ongadi, E. L. Huskins, and B. C. Walker, Phys. Rev. Lett. **94**, 243003 (2005).
[25] M. Verschl, Laser Phys. **18**, 598 (2008).
[26] M. Verschl and C. H. Keitel, J. Phys. B **40**, F69 (2007).
[27] N. Milosevic, P. B. Corkum, and T. Brabec, Phys. Rev. Lett. **92**, 013002 (2004).
[28] P. D. Grugan, S. Luo, M. Videtto, C. Mancuso, and B. C. Walker, Phys. Rev. A **85**, 053407 (2012).
[29] H. Li, J. Chen, H. Jiang, P. Fu, J. Liu, Q. Gong, Z.-C. Yan, and B. Wang, Phys. Rev. A **83**, 013408 (2011).
[30] M. Drouin, L. Gremillet, J.-C. Adam, and A. Héron, J. Comput. Phys. **229**, 4781 (2010).
[31] A. Pukhov, J. Plasma Phys. **61**, 425 (1999).
[32] S. L. Haan, Z. S. Smith, K. N. Shomsky, and P. W. Plantinga, J. Phys. B **42**, 134009 (2009).
[33] J. D. Jackson, *Classical Electrodynamics* (John Wiley and Sons, Hoboken, NJ, 1998).
[34] A. N. Kaufman and P. S. Rostler, Phys. Fluids **14**, 446 (1971).
[35] H. A. Bethe and E. E. Salpeter, *Quantum Mechanics of One- and Two-Electron Atoms* (Springer-Verlag, Berlin, 1957).
[36] F. Mauger, C. Chandre, and T. Uzer, Phys. Rev. Lett. **102**, 173002 (2009).
[37] G. Sansone, C. Vozzi, S. Stagira, and M. Nisoli, Phys. Rev. A **70**, 013411 (2004).
[38] N. Milosevic, V. P. Krainov, and T. Brabec, Phys. Rev. Lett. **89**, 193001 (2002).